Influence of Confined Polymer Structure on Proton Transport Property in Sulfonated Polyimide Thin Films

Karthik KRISHNAN,[a] Tomoaki YAMADA,[b] Hiroko IWATSUKI,[c] Mitsuo HARA,[c] Shusaku NAGANO,[d] Kazuya OTSUBO,[e] Osami SAKATA,[f] Akihiko FUJIWARA,[g] Hiroshi KITAGAWA,[e] Yuki NAGAO[a,*]

[a] School of Materials Science, Japan Advanced Institute of Science and Technology, 1-1 Asahidai, Nomi, Ishikawa 923-1292, Japan.

[b] Department of Materials, Physics and Energy Engineering, Nagoya University, Furo-cho, Chikusa, Nagoya 464-8603, Japan

[c] Department of Molecular Design & Engineering, Graduate School of Engineering, Nagoya University, Furo-cho, Chikusa, Nagoya 464-8603, Japan

[d] Nagoya University Venture Business Laboratory, Nagoya University, Furo-cho, Chikusa, Nagoya 464-8603, Japan

[e] Division of Chemistry, Graduate School of Science, Kyoto University, Kitashirakawa Oiwake-cho, Sakyo-ku, Kyoto 606-8502, Japan

[f] Synchrotron X-ray Station at SPring-8, National Institute for Materials Science (NIMS), 1-1-1 Kouto, Sayo-cho, Sayo-gun, Hyogo 679-5148, Japan

[g] Japan Synchrotron Radiation Research Institute (JASRI), SPring-8, 1-1-1 Kouto, Sayo-cho, Sayo-gun, Hyogo 679-5198, Japan

*Corresponding author: ynagao@jaist.ac.jp

Abstract

The organized structure and proton transport property in sulfonated polyimide (SPI) thin film have been studied, much less is known at the interfacial charge transport during confinement of such materials. The proton conductivity of SPI thin film is correlated well with the highly oriented polymer structures as determined by infrared (IR) p-polarized multiple-angle incidence resolution spectrometry (p-MAIRS) and *in situ* RH dependent synchrotron grazing incidence X-ray diffraction (GI-XRD). The high proton conductivity of 2.8×10^{-1} S cm^{-1} at 80 ºC and 90% RH was achieved in the highly oriented SPI thin film. In contrast, the bulk SPI showed the drop of conductivity value at high relative humidity region, which is due to the significant structural disorder accompanied by the strong interaction between the sulfonic acid side chains and water molecules.

Keywords

Conductivity enhancement, Confined polymer thin film, Organized structure

1. Introduction

Molecular nano-structure organizations have grown in importance for efficient ionic transportation.[1-4] Especially, molecular orientation and interfacial structure in the nanostructured materials have been an active area of research for proton transportation in fuel cell applications.[5-7] In polymer ultrathin films, the interfacial confinement at the polymer-substrate boundary and free surface effects causes the specific interaction between the adjacent polymer chains, which results the distinct polymer properties relative to that of bulk materials.[8] For instance, in our previous studies, we observed the enhancement of proton conductivity in pyromellitic dianhydride based sulfonated polyimide (PMDA/SPI) thin film when the films confined into the nanoscale regime. Owing to the interfacial polymer chain confinement in the in-plane direction favors the formation of long-range proton conduction path and thus exhibited the high proton conductivity.[9] Consequently, the preferred chain packing along the in-plane/out-of-plane direction in the confined film could be an additional impact for forming the macroscopic proton transport path as like proton wires to improve the charge transport characteristics in proton exchange membrane fuel cells (PEMFCs).[10,11] Therefore, achieving the directed assembly of polymer chains in thin films has attracted intense interest in recent years.[12,13]

Many investigations concerning the relationship between chemical structures and application performances for polyimide (PI) systems are devoted because the chemical structure of PI is one of the essential factors associated with the secondary and tertiary structures and the physical properties.[14-16] For PEMFC applications, the sulfonated polyimides have received much attention due to its excellent thermal, chemical, mechanical stability and resistive to swelling.[17-19] In particular, the PI based systems have been prepared using the sulfonic acid groups as side chains

directly bound to the polymer backbone.[20,21] This has led to the hydrolytic stability and it greatly depends on the basicity of the amido nitrogen. Also, the enhancement of hydrolytic stability can be possible when the spacer group is positioned in between the $–SO_3H$ group and phenyl ring.[22] In general, the sulfonated groups in the polymer electrolyte exhibit excessive swelling under fully hydrated conditions, which deteriorates the performance of fuel cell operation. Therefore, a number of structural investigations have been done on SPI to improve the proton conductivity and stability profiles of SPIs.[23,24]

This work elucidates the relationship between polymer orientation and proton transport characteristics in SPI systems. The p-MAIRS[25,26] and *in situ* RH dependent synchrotron GI-XRD were taken into account to investigate the polymer orientation and internal structure when confined into thin film. The diffraction patterns of SPI film can be attributed to the lamellar structure falls parallel to the substrate; in addition, the ordering of lamellar phase significantly varies with the humidity change. The impedance studies under both RH and temperature dependent were used to characterize the proton transport property in SPI. This insight has the potential to understand more clearly on the structure-property relation in such systems.

2. Experimental

2.1. Materials

3,3'-Dihydroxybenzidine, propanesultone, and 1,4,5,8-Naphthalenetetracarboxylic dianhydride (NTDA) were used as received from TCI, Japan and Sigma–Aldrich, respectively. Acetic acid, acetic anhydride, nitric acid, methanol, ethanol and acetone were purchased from Wako Chemicals, Japan. Hydrochloric acid (Nacalai Tesque, Japan), sodium hydroxide (Kishida

Chemical, Japan), m-cresol, and triethylamine (TEA) (Kanto Chemicals, Japan) were used as received.

2.2. Synthesis of sulfonated diamine monomers

Scheme 1 represents the steps involved in preparing of the sulfonated naphthalenic polyimides. The reaction starts with the mixtures of 3,3'-dihydroxybenzidine (5 g) acetic acid (1.5 ml), acetic anhydride (79 ml) and distilled water (200 ml). Subsequently, this reaction mixture was stirred at 70 °C for 1 hr. The obtained precipitates were washed several times with cooled acetone and separated using centrifugation. Presence of modified acetyl functional group was confirmed by using ^{1}H NMR. Then, the sulfonation was carried out using acetylated 3,3'-dihydroxybenzidine, propanesultone (7.3 g), sodium hydroxide (2.4 g) and methanol (150 ml). The mixed products were refluxed constantly at 80 °C under an inert atmosphere for 6 hr. Obtained final precipitates were washed with cold methanol to remove the unreacted species. Then, the sulfonated monomers were dissolved in water to precede the ion-exchange process (using Amberlyst). For removing the acetate group, we used the concentrated hydrochloric acid (HCl) to the ion-exchanged sulfonated product. Refluxing was conducted at 120 °C for 1 hr under an inert atmosphere. After the mixture was refluxed, HCl was evaporated at 150 °C; in addition, the HCl vapor was carefully neutralized with a concentrated base. Prior to each step, all of the prepared monomers were characterized by ^{1}H NMR. The degree of sulfonation for the final product was estimated from ^{1}H NMR data and it is more than 96%. The calculated ion exchange capacity is ~2.8 mequiv/g.

2.3. Synthesis of Sulfonated naphthalenic polyimides

The sulfonated monomers (1 mol) were polymerized with the required amount of NTDA (1 mol), m-cresol (5 ml), and TEA (0.3 ml). m-Cresol was used as solvent, and the polymerization

reaction was carried out under an inert atmosphere at 150 °C for 5 hr. The polymerized product was collected after being washed with cooled acetone. The final product was obtained by an ion-exchange process at least 8 times using a mixture solution of concentrated nitric acid and ethanol (1/12 by volume). The obtained product was washed with ethanol and dried in vacuumed desiccator. GPC measurement was used to estimate the molecular weight of the prepared polymer, which was found to be 1.5×10^5.

2.4. Preparation of thin films

SPI thin film on quartz substrate was prepared using an Active ACT−200 spin-coater. Prior to film deposition, the substrate was subjected to several cleaning processes, and plasma treatment was performed using a vacuum plasma system (Cute-MP; Femto Science, Korea) to improve surface hydrophilicity. The thickness of the thin film was measured using a surface profiler (KLA-Tencor P-15 profiler).

2.5. Conductivity measurements of the thin films

Proton conductivity was estimated through impedance spectroscopy measurements using a Solartron 1260 frequency response analyzer equipped with a high-frequency Solartron 1296 dielectric interface. The relative humidity (RH) and temperature were established using a computer-controlled environmental test chamber (SH-221; Espec Corp). The conductivity measurements were performed at 298 K and at various RH values. For the thin film measurements, the electrode configuration was selected to obtain measurements of the current flow in the plane parallel to the substrate surface and two-probe method was employed to obtain the impedance data. Gold contacts were used as the thin film electrodes for the conductivity measurements. The impedance data were collected between the frequency range of 1 Hz and 10

MHz, with an applied alternating potential of 50 mV. Thin-film conductivity (σ) was estimated by the following relation,

$$\sigma = \frac{d}{Rlt} \tag{1}$$

where *d* is the distance between the gold electrodes, *R* is the resistance value obtained directly from the impedance measurement, *l* is the length of the contact electrodes, and t is the thickness of the film (Figure 1).

2.6. p-Polarized multiple angle incidence resolution spectrometry (p-MAIRS)

The polymer orientation in thin films has been studied using p-MAIRS. The Si wafers was used as substrate and the surface of the original Si wafer was oxidized before the measurement. The p-MAIRS measurements were obtained with a Fourier-transform infrared (FTIR) spectrometer (Nicolet 6700; Thermo−Fisher Scientific) equipped with a mercury cadmium telluride (MCT) detector. The single-beam spectra were collected from 38° to 8° in 6° steps between the angle of incidence.

2.7. Fourier-transform infrared attenuated total reflectance (FTIR-ATR**)**

The bulk SPI has been studied using FTIR-ATR. The spectrum was obtained with a Fourier-transform infrared (FTIR) spectrometer (Nicolet 6700; Thermo−Fisher Scientific) equipped with a deuterated triglycine sulfate (DTGS) detector and an optional SMART iTR. Sample was pelletized, and then the flat surface of the pellet was used for the ATR measurement.

2.8. The *in situ* synchrotron grazing incidence X-ray diffraction (GI-XRD)

The XRD measurements at a fixed grazing incident angle (α) for thin films were carried out with various relative-humidity (RH) at room temperature using a six-axis diffractometer installed at a BL13XU beamline in SPring-8 (Japan Synchrotron Radiation Research Institute, Hyogo,

Japan). The incident angle (α) was set to 0.4º. RH was controlled by BEL-Flow apparatus (BEL Japan, Japan). The wavelength (λ) of the radiation used in this experiment was equal to 0.1550 nm. The data were collected as α-2θ mode in 1 s as step time and the 2θ step angle was 0.2º with a NaI(Tl) scintillation detector.

3. Results and discussion

The difference in proton conductivity between the pelletized bulk SPI (0.40 mm) and thin film (1.0 μm) have been studied using both RH and temperature dependent measurements. Figure 2 represents the RH dependent proton conductivity plots for both bulk SPI and thin film cases. It can be clearly seen that the Log conductivity increases linearly up to 95% RH in SPI thin film, unlike the bulk SPI. The conductivity drops appeared at after 80% RH in the bulk SPI sample. The strong interaction between the water molecules and sulfonated groups in SPI polymer chains under high humidified condition causes the structural instability, which may be due to the origin of excessive swelling. This structural instability exhibits the drop of conductivity at high humidity range. The maximum proton conductivity is achieved in the SPI thin film (2.0×10^{-1} S cm^{-1}, at 95% RH and 298 K), which is nearly one order of magnitude higher than the conductivity of bulk SPI (1.2×10^{-2} S cm^{-1}, at 80% RH and 298 K). It is anticipated that the specific interaction between the polymer chain at interfaces in thin film regime influence the variation of proton conductivity than bulk sample.

The temperature dependent proton conductivity plots with a constant RH of 90% for both bulk SPI and thin film are shown in Figure 3. It is observed that the proton conductivity increases with the increase in temperature and reaches its maximum value (2.8×10^{-1} S cm^{-1} at 80 ºC) in the SPI thin film. On the other hand, the proton conductivity of bulk SPI shows the value of 9.8

$\times 10^{-3}$ S cm^{-1} at 50 ºC, which is almost one order of magnitude lower than the SPI thin film (2.2 $\times 10^{-1}$ S cm^{-1} at 50 ºC). Similar observation has already been reported to be the value of proton conductivity of SPIs in water were around 2.0 $\times 10^{-1}$ S cm^{-1} at 50 ºC and RH above 80%, which is due to the high ion exchange capacity and high water uptake capability accompanied with the water stability.[20] But, the results presented in this work shows the enhanced proton conductivity value than the previous report. Because, the thin film confinement at nanoscale regime can be responsible for obtaining both the enhanced structural stability and proton conductivity. It is also expected that the large scale interrupted domains in the randomly oriented bulk SPI cannot leads to the long-range proton transport path, which possibly disrupt the fast ion conduction (Figure 4). According to the Arrhenius equation (2), the activation energy (E_a) was estimated and the values for the bulk SPI and thin film are 0.11 eV and 0.10 eV, respectively.

$$\sigma T = \sigma_0 \, exp\left(\frac{-E_a}{RT}\right) \quad (2)$$

where E_a, R, T and σ_0 represents the activation energy, gas constant, temperature and pre-exponential factor, respectively. The conductivity patterns are quite similar with our previous observation in the PMDA/SPI samples.[9]

The infrared p-MAIR spectroscopy used in this investigation is an important tool for the identification of molecular orientation in thin films. Thereby, the in-plane (IP) and out-of-plane (OP) SPI orientation in thin film has been investigated using p-MAIRS (Figure 5). The typical naphthalimide absorption bands were observed at 1716, 1676 and 1349 cm^{-1}, which corresponds to the symmetric, asymmetric vibrations of C=O groups and vibration of C−N group of the six-membered imide rings, respectively. The observed broad band at 1248 and 1195 cm^{-1} corresponding to the asymmetric and symmetric vibration of O=S=O in the sulfonic acid

groups.[27,28] The polymer orientation in SPI thin film has been distinguished according to the changes in the intensity of p-MAIR spectra. In principle, the maximum intensity of the p-MAIR signal arise when the electric field vector of IR rays and the orientation of the molecular vibration are parallel.[29] Consequently, the IP vibrational modes of C=O and C−N groups are approximately two times stronger intensity than the OP component, revealing that the SPI thin film makes the highly oriented structure parallel to the substrate plane. Furthermore, there is noticeable peak shift to the higher wavenumber region (1680 cm^{-1}) is found in the C=O asymmetric mode[27,28] of OP component relative to that of the IP component (1676 cm^{-1}). The band shift in the p-MAIR spectra is regarded due to the Berreman effect.[30,31] Also, this high wavenumber shift suggests that the longitudinal mode may contributes a slight surface perpendicular component.[32]

In the bulk SPI, the FTIR-ATR measurement was done and the characteristic vibrational modes are shown in Figure 6. Owing to the random orientation of the bulk SPI, consideration of the intensity of vibration mode is insignificant for investigation. It is also essential to mention that the frequency downshift is observed for both the asymmetric C=O (1711 cm^{-1})[27] and symmetric C=O (1666 cm^{-1}) stretching vibrations of bulk SPI than that of the stretching modes in oriented film.

The change in internal polymer structure and crystalline order of the SPI thin film was determined by *in situ* RH dependent synchrotron GI-XRD and thereby correlating with the proton transport property. Figures 7(a) and 7(b) shows the diffraction pattern and *d*-spacing values for SPI thin film with various RH conditions. The measurement has been taken only in the out-of-plane direction and it plays a vital role for understanding the variation in the molecular structure with the change in RH. Essentially, the 1D GI-XRD pattern shows the shift in peak

position towards the lower angle region with the increase in RH. Initially (at 0% RH), the peak is located at 7.1º (2θ) and it tends toward the lower angle region with the value of 4.6º at fully hydrated region (at 95% RH). The corresponding *d*-spacing values for these two peaks are 1.25 nm and 1.93 nm, respectively. This large deviation in the polymer structure is due to the perturbed interlamellar stacking in the out-of-plane direction by the introduction of water molecules. Also, it suggests that the spacing between the interlamellar stacking increases with the increase in RH, which reasons the shift in peak position. To gain further insight into the effect of RH in the SPI thin film, the relative intensity of the diffraction pattern must be considered. The relative intensity of the diffraction increases gradually with an increase in the RH. This implies that the degree of crystallinity improved by RH and causes the aggregated structures such as liquid-crystal-like and ordered crystalline structures.[33] The increase in humidity results the remarkable interaction between the aggregated lamellar structures and water molecules, which possibly rearranged the crystalline order. Understanding of this structural property well correlates with our earlier finding of the expansion of lamellar structure in the out-of-plane direction when the PMDA/SPI system hydrated fully.[9] The aggregation and oriented molecular structure in SPI thin films have been investigated; in addition, the strong intermolecular interaction reasons the higher degree of spontaneous chain orientation, which could improve the performance properties of polymer electrolytes. For instance, some reports were evidenced that the oriented PI structures parallel to substrate plane could an additional impact for the improving the physical properties, such as birefringence and thermal expansion coefficient.[34,35] Mostly, the rigid and planar PI molecular structures can be responsible for the higher degrees of in-plane orientation than those having bent and three dimensional molecular structures.[33]

This study reveals that the organized structure in SPI thin film significantly exhibit the high proton conduction. The chemical stability also plays an essential role in obtaining the high proton conduction, which derived from the spacing between the sulfonic acid group and polyimide main chain. Furthermore, the lyotropic lamella structure parallel to the substrate plane formed the long-range proton transport path when the SPI confined into film. As mentioned in the previous studies,[14,33,36] the planar PI molecular structure mostly orients the polymer chain in the in-plane direction, which possibly enhances the proton conductivity in such thin film system.

4. Conclusions

The significance of molecular orientation on the proton transport property in sulfonated naphthalenic polyimide thin film was studied using p-MAIRS and *in situ* RH dependent synchrotron GI-XRD. The p-MAIR spectra disclose the highly oriented polymer structure in the IP direction when the SPI polymer confined into thin film, whereas the bulk SPI showed randomly oriented polymer structure, confirmed by FTIR-ATR. Hydration effect on the interlamellar stacking influenced the variation of diffraction patterns in GI-XRD. It is speculated that the specific interaction between the water molecules and side chain sulfonic acid groups in SPI rearranged the molecular structure in the out-of-plane direction, can be termed as a lyotropic liquid-crystal-like phase. Furthermore, the enhancement of crystalline order with an increase in RH can be due to the ch-packing between the continuous polyimide chains aligns more readily on the out-of-plane direction. As consequence, the highly oriented polymer structure in SPI thin film influenced the enhancement of proton conductivity, which exhibits one order of magnitude more conductivity value than the randomly oriented bulk SPI system. These structure-property relationships promise to assist in the development of fuel cell performance with rationally designed highly oriented polymer materials and enhanced proton transport properties.

Acknowledgments

Synchrotron XRD measurements were supported by the Japan Synchrotron Radiation Research Institute (JASRI) (Proposal No.: 2012A1072). This work was financially supported by the Japan Society for the Promotion of Science (JSPS) through the Funding Program (GR060) for Next Generation World-Leading Researchers (NEXT Program), initiated by the Council for Science and Technology Policy (CSTP). This work was partially supported by the Ogasawara Foundation for the Promotion of Science and Engineering.

References

1. J. Ruokolainen, R. Makinen, M. Torkkeli, T. Makela, R. Serimaa, G. ten Brinke, and O. Ikkala, *Science*, **280**, 557 (1998).
2. T. Kato, N. Mizoshita, and K. Kishimoto, *Angew. Chem. Int. Ed*., **45**, 38 (2006).
3. B. Soberats, M. Yoshio, T. Ichikawa, S. Taguchi, H. Ohno, and T. Kato, *J. Am. Chem. Soc*., **135**, 15286 (2013).
4. T. Tamura and H. Kawakami, *Nano Lett.*, **10**, 1324 (2010).
5. J. Matsui, H. Miyata, Y. Hanaoka, and T. Miyashita, *ACS Appl. Mater. Interfaces*, **3**, 1394 (2011).
6. Y. Nagao, J. Matsui, T. Abe, H. Hiramatsu, H. Yamamoto, T. Miyashita, N. Sata, and H. Yugami, *Langmuir*, **29**, 6798 (2013).
7. A. Kongkanand, *J. Phys. Chem. C*, **115**, 11318, (2011).
8. S. K. Dishari, and M. A. Hickner, *Macromolecules*, **46**, 413 (2013).
9. K. Krishnan, H. Iwatsuki, M. Hara, S. Nagano, and Y. Nagao, *J. Mater. Chem. A*, **2**, 6895 (2014).
10. M. A. Modestino, D. K. Paul, S. Dishari, S. A. Petrina, F. I. Allen, M. A. Hickner, K. Karan, R. A. Segalman, and A. Z. Weber, *Macromolecules*, **46**, 867 (2013).
11. J. Li, K. Kamata, M. Komura, T. Yamada, H. Yoshida, and T. Iyoda, *Macromolecules*, **40**, 8125 (2007).
12. O. Kim, G. Jo, Y. J. Park, S. Kim, and M. J. Park, *J. Phys. Chem. Lett*., **4**, 2111 (2013).
13. J. Li, K. G. Wilmsmeyer, and L. A. Madsen, *Macromolecules*, **41**, 4555 (2008).
14. T. P. Russell, H. Gugger, and J. D. Swalen, *J. Polym. Sci*., **21,** 1745 (1983).

15. Y. Xiao, T. Chung, M. L. Chng, S. Tamai, and A. Yamaguchi, *J. Phys. Chem. B*. **109**, 18741 (2005).

16. S. Numata, and T. Miwa, *Polymer*, **30**, 1170 (1989).

17. J. Fang, X. Guo, S. Harada, T. Watari, K. Tanaka, H. Kita, and K. Okamoto, *Macromolecules*, **35**, 9022 (2002).

18. K. Miyatake, N. Asano, and M. Watanabe, *J. Polym, Sci., Part A: Polym. Chem.*,**41**, 3901 (2003).

19. X. Ye, H. Bai, and W. S. W. Ho, *J. Membr. Sci*., **279**, 570 (2006).

20. Y. Yin, Y. Suto, T. Sakabe, S. W. Chen, S. Hayashi, T. Mishima, O. Yamada, K. Tanaka, H. Kita, and K. Okamoto, *Macromolecules*, **39**, 1189 (2006).

21. N. Asano, M. Aoki, S. Suzuki, K. Miyatake, H. Uchida, and M. Watanabe, *J. Am. Chem. Soc*., **128**, 1762 (2006).

22. O. Savard, T. J. Peckham, Y. Yang, and S. Holdcroft, *Polymer*, **49**, 4949 (2008).

23. Y. Yin, J. Fang, T. Watari, K. Tanaka, H. Kita and K. Okamoto, *J. Mater. Chem*., **14**, 1062 (2004).

24. N. Asano, K. Miyatake and M. Watanabe, *Chem. Mater*., **16**, 2841 (2004).

25. T. Hasegawa, *J. Phys. Chem. B*, **106**, 4112 (2002)**.**

26. T. Hasegawa, *Anal. Chem*., **79**, 4385 (2007)**.**

27. K. Chen, Z. Hu, N. Endo, M. Higa, and K. Okamoto, *Polymer*, **52**, 2255 (2011).

28. C. Liu, L. Li, Z. Liu, M. Guo, L. Jing, B. Liu, Z. Jiang, T. Matsumoto, and M. D. Guiver, *J. Memb. Sci*., **366**, 73 (2011).

29. T. Hasegawa, *Anal. Bioanal. Chem*., **388**, 7 (2007).

30. D. W. Berreman, *Phys. Rev.*, **130**, 2193 (1963).

31. T. Hasegawa, *J. Phys. Chem. B,***106**, 4112 (2002).

32. M. Matsunaga, T. Suzuki, K. Yamamoto, and T. Hasegawa, *Macromolecules*, **41**, 5780 **(**2008**)**.

33. J. Wakita, S. Jin, T. J. Shin, M. Ree and S. Ando, *Macromolecules*, **43**, 1930 (2010).

34. Y. Terui, and S. Ando, *J. Polym. Sci., Part B,* **42**, 2354 (2004).

35. M. T. Pottiger, J. C. Coburn, and J. R. Edman, *J. Polym. Sci., Part B,* **32**, 825 (1994).

36. T. P. Russell, *J. Polym. Sci*., **22,** 1105 (1984).

Scheme caption

Scheme 1. Synthesis of sulfonated naphthalenic polyimides

Figure caption

Figure 1. Schematic representation of highly oreinted thin film used to measure in-plane proton conductivity.

Figure 2. RH dependent proton conductivity plots for both the pelletized bulk SPI and thin film.

Figure 3. Arrhenius plots of conductivity for both the pelletized bulk SPI and thin film.

Figure 4. (a) Proposed structure of the long range proton transfer path in the highly oriented SPI interfacial structure and (b) interrupted domains in the randomly oriented bulk SPI

Figure 5. Infrared p-MAIR spectra for the SPI thin film, measured from 38° to 8° in steps of 6°.

Figure 6. FTIR-ATR spectrum for the bulk SPI.

Figure 7. (a) diffraction patterns and (b) the estimated *d*-spacing values of SPI thin film with various RH using *in situ* synchrotron GI-XRD.

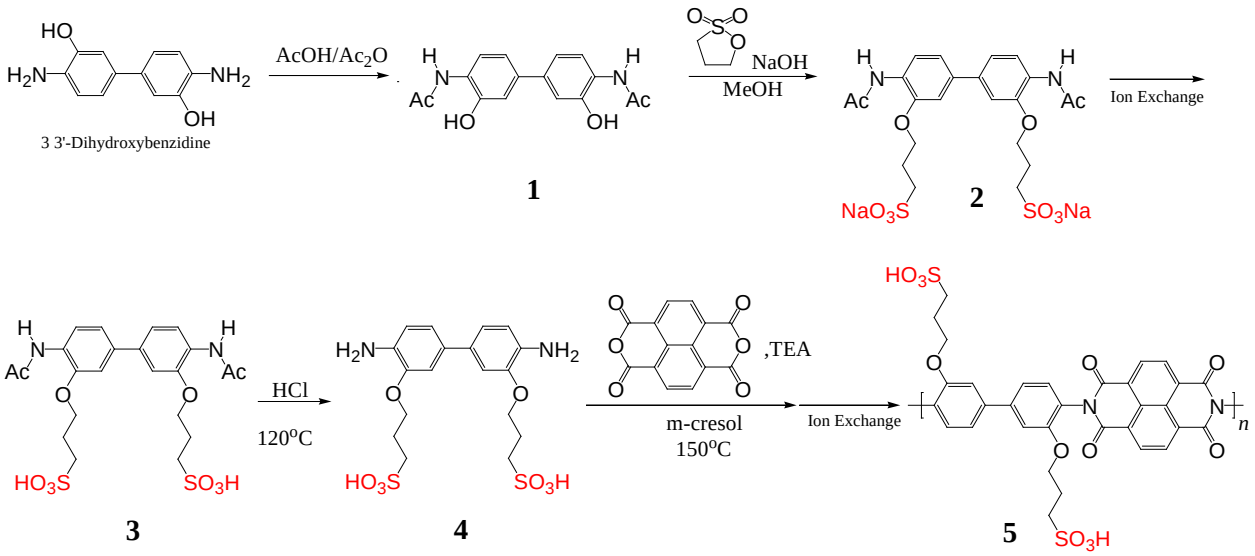

Scheme 1. K. Krishnan *et al.*

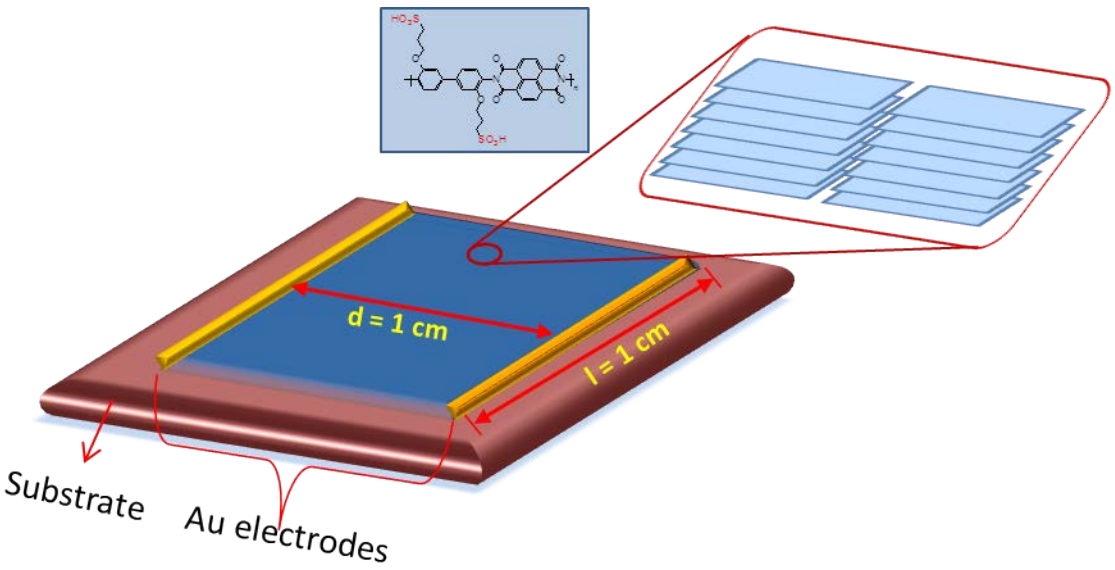

Figure 1. K. Krishnan *et al.*

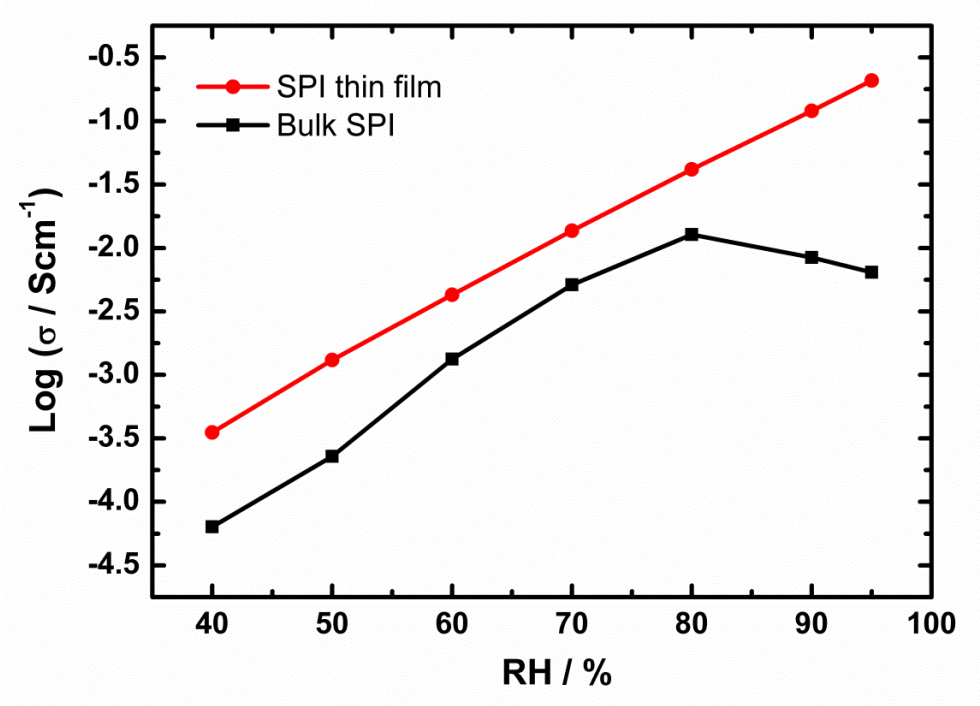

Figure 2. K. Krishnan *et al.*

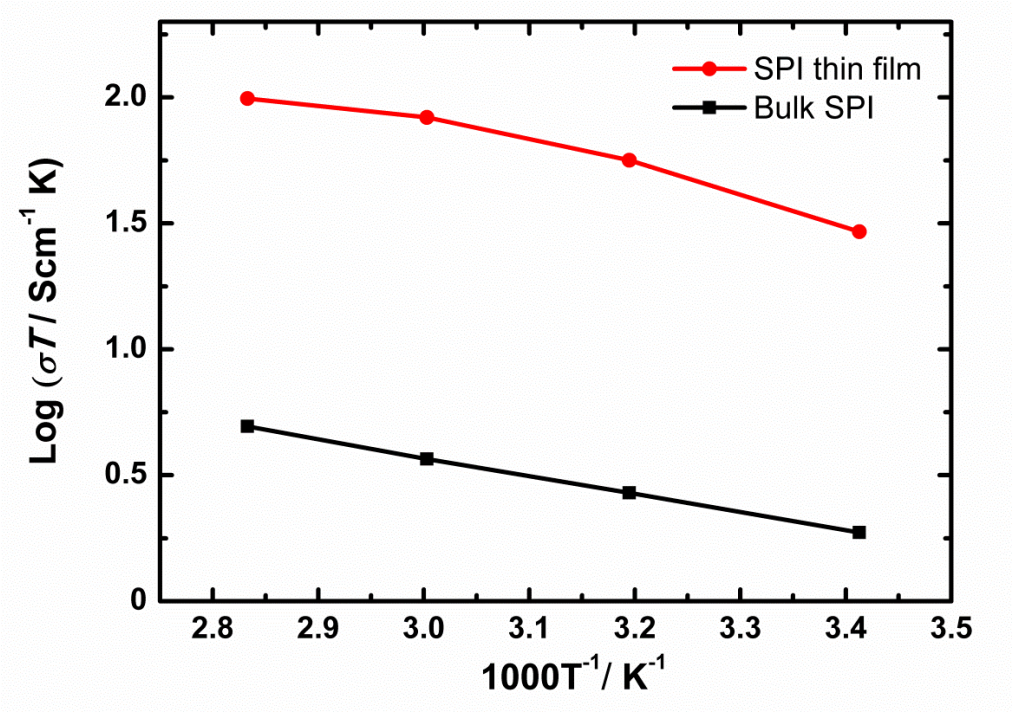

Figure 3. K. Krishnan *et al.*

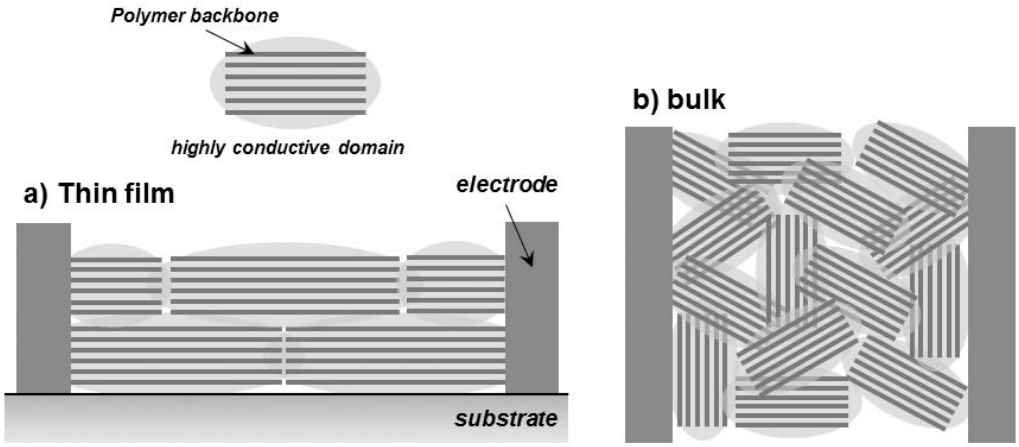

Figure 4. K. Krishnan *et al.*

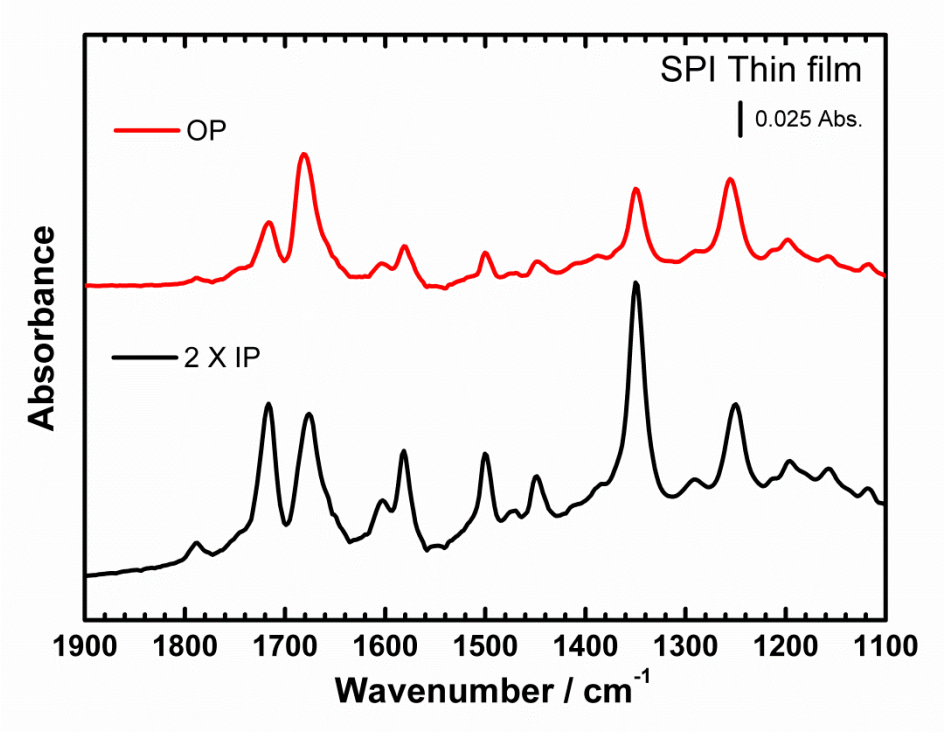

Figure 5. K. Krishnan *et al.*

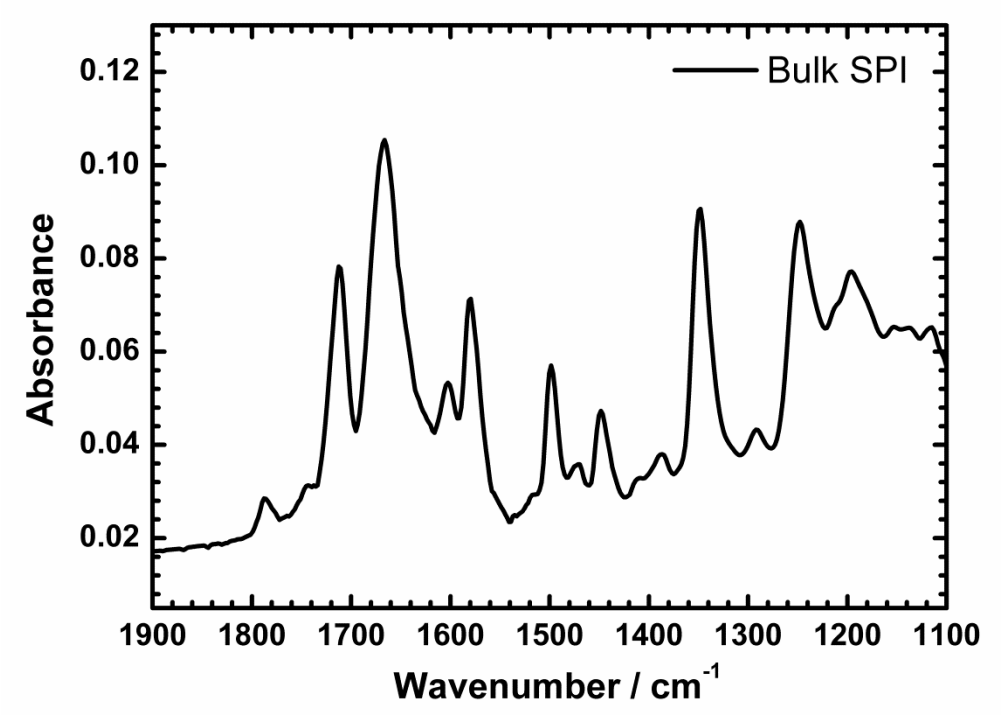

Figure 6. K. Krishnan *et al.*

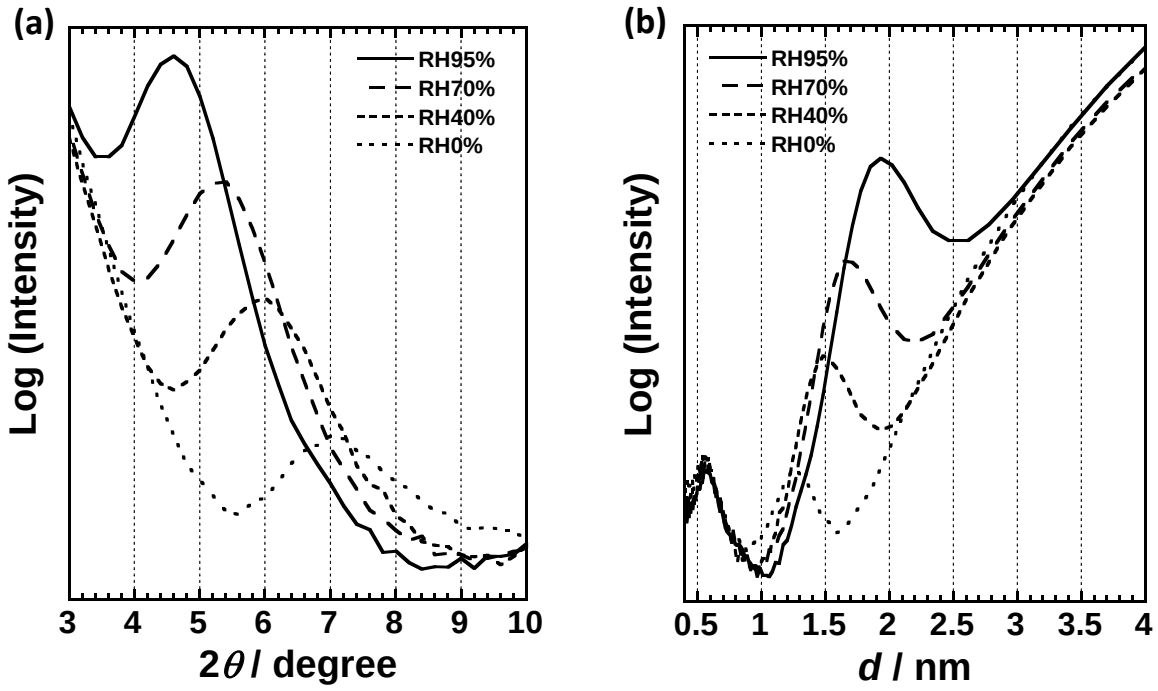

Figure 7. K. Krishnan *et al.*